Nitrogen-terminated milled nanodiamond surfaces by plasma exposure

Mohan Kumar Kuntumalla, Arsène Chemin, Marie Finas, Hugues Girard, Shaul Michaelson, Tristan Petit, Jean-Charles Arnault, Alon Hoffman

Nitrogen-Terminated Milled Nanodiamond Surfaces by Plasma Exposure

Mohan Kumar Kuntumalla[a]*, Arsène Chemin[b], Marie Finas[c], Hugues A. Girard[c], Shaul Michaelson[a], Tristan Petit[b], Jean-Charles Arnault[c] and Alon Hoffman[a]**

a Schulich Faculty of Chemistry, Technion−Israel Institute of Technology, Haifa, 32000, Israel

b Helmholtz-Zentrum Berlin für Materialien und Energie, Hahn-Meitner-Platz 1, 14109, Berlin, Germany

c Université Paris-Saclay, CEA, CNRS, NIMBE, 91191 Gif sur Yvette, France

*Email: kmohan-kumar@technion.ac.il

**Email: choffman@technion.ac.il

Phone: +972 48293747

Keywords: Nanodiamond; Nitrogen termination; Nitrogen plasma; X-ray photoelectron spectroscopy; High resolution electron energy loss spectroscopy; Near-edge X-ray absorption fine structure

Abstract

This study investigates surface modifications of hydrogen-terminated milled nanodiamond (H-MND) drop-casted films by microwave (MW) and radio frequency (RF) nitrogen plasma exposures. The RF(N_2) damaging plasma treatment results in the highest nitrogen adsorption (~7.5 at.%), followed by MW(N_2) (~4.2 at.%) and RF(N_2) non-damaging (~3.8 at.%) plasma treatments. Upon MW(N_2) plasma exposure, nitrogen predominantly adsorbs in C–N/C=N and NH states, whereas RF(N_2) treatments result in mixed C–N/C=N, C≡N, and NH states, as revealed by electron spectroscopy. Crystalline edges strongly influence the N, H, and O adsorption onto MND and act as active adsorption sites. The NH(ads) concentration is notably higher on MND surfaces compared to on poly/single-crystalline surfaces, likely favored by the additional bonding configuration of hydrogen on the MND. NH(ads) species desorbed upon vacuum annealing in the 500-700 °C range, leaving a CN adsorbed species onto the MND surfaces. The nitrogen and oxygen concentration monotonically decreases with annealing temperature from 300 to 1000 °C. Upon high-temperature annealing, partial recovery of the MND surfaces occurs depending on plasma exposure conditions. This study may be critical in

all ex-situ applications influenced by the near-surface physicochemical and electronic properties of nitrogen-terminated MND surfaces, such as NV centers in nanocrystals.

1. Introduction

Surface properties of diamond nanoparticles or nanodiamonds (ND) are expected to vary depending on the production process, resulting in well-faceted or round particles of different sizes of different chemical and phase compositions.[1] Milled nanodiamonds (MND) from bulk HPHT, CVD, or natural diamond display faceted surfaces of different orientations with high crystallinity, whereas detonation nanodiamonds (DND) have rounded shapes, low crystallinity and are embedded within a C(sp^2) shell. These differences are expected to result in different surface properties, as reported in recent studies on MND and DND.[2] Therefore, both materials may be selectively employed for specific applications, such as, spin properties of MND (containing color centers) may be utilized for quantum applications.[3] It is suggested that nitrogen-vacancy (NV^-) centers in MND may be used for local nanoprobes as their surfaces display high crystallinity similar to polycrystalline diamond. Recent studies underlined that the surface electronic properties (surface conductivity and negative electron affinity), well-known for hydrogenated single and polycrystalline diamonds, are also surface assets of hydrogenated-MND (H-MND).[4, 5] The H-MND surface characteristics may resemble bulk diamond upon proper surface terminations.[6] We have recently reported that nitrogen termination of Diamond (100) surfaces by an RF(N_2) plasma under specific conditions enhances near-surface NV^- properties.[7] Therefore, it is expected that the chemical termination of the MND surfaces by nitrogen bonding using a similar plasma procedure would also result in the preferred population of their near-surface NV^- centers. Motivated by these results, in this study, we investigated the possibility of nitrogen terminating the surfaces of H-MND particles by different nitrogen plasmas exposures, as previously reported in our polycrystalline and oriented single crystalline diamond surfaces studies.[8-13] Nitrogen termination of H-MND surfaces may be necessary to enhance NV^- centers embedded within these nanodiamond particles for quantum sensing applications.[14]

In this paper, we present our surface studies on nitrogen and oxygen bonding, concentration, and thermal stability up to 1000 °C by ex-situ X-ray photoelectron spectroscopy (XPS) and high resolution electron energy loss spectroscopy (HREELS) onto drop-casted H-MND films exposed to RF and MW nitrogen plasmas. The oxygen co-adsorption upon exposure of the nitrogen-terminated H-MND surfaces to ambient conditions is an important aspect to consider, as in most applications, it may affect the electronic properties of such surfaces. The H-MND

structural characterization of the H-MND particles by transmission electron microscopy (TEM) is presented in Section-S1 in supporting information (SI). TEM analysis presents the well-faceted structure of the H-MND particles and their size distribution. In addition, a comparison of some surface properties related to hydrogen bonding of the H-MND to those of H-PCD and H-Di(100) investigated by near-edge X-ray absorption fine structure measurements (NEXAFS), XPS, and HREELS is presented in Section-S2 in SI. In the case of HREELS, we also present spectra measured for the H-Di(111) surface. By this, we attempt to rationalize the nature of the nitrogen bonding to the H-MND and compare it to those of H-PCD, H-Di(111), and H-Di(100) surfaces.

2. Methods

2.1. Drop-Casted H-MND Film Preparation

The drop-casted H-MND film preparation is described briefly. Milled nanodiamonds (from Van Moppes (SYP 0-0.05)) were used to prepare the drop-casted H-MND films previously described.[5] Nanoparticles were first oxidized by annealing under air (P_{atm}, 480 °C for 5 h). Then, hydrogenation of oxidized MND was achieved by annealing under H_2 (P_{atm}, 50 sccm, 750°C for 5 h) with a first desorption step at 200 °C for 30 min. Aqueous suspension was prepared by sonication followed by centrifugation. For sonication, 100 mg of powder was disposed in a 15 mL plastic tube filled with 2.5 mL of ultrapure water (18.2 MΩ.cm). A Cup Horn Bioblock Scientific 750 W system was used with a cooling system at 10 °C throughout the ultrasonic treatment. Sonication was realized for 30 min with a 1 s on/off period. Centrifugation was performed during 40 min at 2400 g. The supernatant was immediately collected at the end of the centrifugation. The suspension was characterized by DLS/zetametry with a Horiba Nanopartica SZ100 system. Acquisitions were realized at 25 °C with a 173° backscattered angle on 0.8 mg/mL supernatant. The distribution of hydrodynamic diameter of H-MND suspended in water was found to be ~30 nm.[5] For sample preparation, 100µL of H-MND suspension (1.75 mg/mL) was drop-casted on 1×1 cm² Si substrate and allowed to dry at ambient temperature.

In addition, the H-PCD, H-Di(100), and H-Di(111) surfaces examined in this study were produced by MW(H_2) plasma exposure and described in detail elsewhere.[9, 11, 13, 15] The structural and morphological characterization of H-MND by electron microscopy and surface chemical characterization by NEXAFS, XPS, and HREELS are presented in Sections -S1 and -S2 in SI.

2.2. Nitrogen Plasma Processes

2.2.1. RF(N_2) Plasma Nitridation

Nitrogen activation was realized using RF and MW sources in separate systems previously described in detail.[15] The RF(N_2) plasma exposures were carried out at N_2 pressures, 3×10^{-2} and 7×10^{-2} Torr, resulting in damaging and non-damaging RF(N_2) plasma nitridation conditions, respectively.[8] Before exposure to the RF(N_2) plasma, the MND samples were in-vacuum annealed to 300 °C to induce weakly bonded ambient adsorbate desorption. Then, the MND samples were exposed to the RF nitrogen plasma at each pressure for 30 min at RT. Following RF(N_2) exposure, the samples were transferred into an ultrahigh vacuum (UHV) equipped with XPS and HREELS analysis facilities under ambient conditions.

2.2.2. MW(N_2) Plasma Nitridation

The MND sample was exposed to MW(N_2) plasma for 15 min, as described in detail elsewhere.[9, 13] Next, the MW(N_2) plasma exposed MND sample was transferred ex-situ into a UHV system for XPS and HREELS analyses.

2.2.3. The Studied Samples

Five H-MND drop-casted films deposited onto silicon substrates were investigated. These samples are:

(i) A drop-casted sample prepared as described in Section-S1 in SI, this sample is termed H-MND as it is expected to be hydrogen terminated by the preparation process and most likely contains some oxygen originating from the sonification process.

(ii) A drop-casted sample followed by a MW(H_2) plasma exposure, as described above before the MW(N_2) plasma exposure. During this MW(H_2) process, the sample temperature was ~200 °C. This sample is termed MW(H_2)-MND.

(iii) A drop-casted H-MND sample after exposure to MW(N_2) plasma.

(iv) A drop-casted H-MND sample after exposure to non-damage RF(N_2) plasma.

(v) A drop casted H-MND sample after exposure to damage RF(N_2) plasma.

2.3. XPS and HREELS Experimental Details

The surface studies were conducted in a UHV system (base pressure of 1×10^{-9} Torr) equipped with XPS and HREELS facilities, as previously described.[8, 16] The wide-range (200-600 eV

binding energy) and narrow spectral ranges (high-resolution) of the N(1s) and C(1s) XP spectra were measured to determine the chemical state of the as-nitrogen terminated surface and stepwise annealed surfaces using pass energy and scan step of 15 eV and 0.1 eV, respectively. Deconvolution of XPS peaks was performed after background subtraction as described by Shirley[17] and using a mixed Gaussian (Y%)-Lorentzian(X%) peak shape, defined in CasaXPS software (version 2.3.15) as GL(X%). HREELS measurements were carried out using a primary electron energy of 8.4 eV. The full width at half maximum (FWHM) of the elastically scattered electron peak was 16 meV. The spectra were recorded up to loss energies of 500 meV in the specular geometry at an incident angle of 55° from the surface normal. The deconvolution of the HREEL spectra was performed utilizing XPSPEAK (version 4.1) software.

3. Results and Discussion

The drop-casted films were transferred ex-situ into the UHV system for XPS and HREELS measurements, performed on the as-prepared samples and subsequently annealed (up to 1000 °C) samples.

The nitrogen and adventitious oxygen concentrations (at.%) in the five samples described above were estimated from the measured wide-range XP spectra in which the O(1s), N(1s), and C(1s) XP peaks could be detected at ~532 eV, ~400 eV and ~285 eV, respectively and depicted in Figure 1(a) and (b). These scans were also performed after stepwise vacuum annealing up to 1000 °C, from which the thermal stability of nitrogen and adventitious oxygen can be determined. These concentrations were estimated using standard sensitivity factors of C, N, and O photoelectrons and assuming a homogenous nitrogen, oxygen, and carbon distribution in the XPS sampled volume.[18] While a natural nitrogen concentration of ~0.3 wt.% was reported in the H-MND particles,[5] no nitrogen was detected on the H-MND films' surfaces by our XPS measurements before the nitrogen plasma exposure procedures. This is expected as the nitrogen concentration is below the detection limit of XPS.

From Figure 1(a), the nitrogen concentration for the RF(N_2) damaging conditions obtains an initial value of ~7.5 at/%, which linearly decreases with annealing temperature till it receives a value of ~1 at.% after annealing to 1000 °C. A similar trend was observed for the RF(N_2) non-damaging conditions with an initial concentration of 3.8 at.% followed by a monotonic decrease up annealing to 1000 °C where a value of ~0.5 at.% was obtained. For the MW(N_2) plasma-treated MND surfaces, an initial value of 4.2 at.% was measured, which was nearly

constant up to an annealing temperature of 500 °C followed by faster decreases at higher annealing temperatures.

The calculated nitrogen concentration obtained after the RF(N_2) damaging conditions exposed H-MND surfaces and their thermal stability follow an intermediate trend as those previously reported for the H-Di(111)[12, 13] and H-Di(100)[10, 11] surfaces. This is as expected, considering that the H-MND are composed of faceted nanocrystallite surfaces. After exposing H-MND to damaging RF(N_2) conditions, the nitrogen concentration was found to be ~7.5 at.%, whereas for the H-Di(111) and H-Di(100) surfaces values of 9.5 and 7.5 at.%, respectively, were obtained. The temperature stability of the incorporated nitrogen, in this case, was intermediate to the H-Di(100) and H-Di(111). This is associated to the higher thermal stability on the H-Di(100) as compared to the H-Di(111) surface.

After exposing the H-MND to RF(N_2) non-damaging and MW(N_2) plasmas, similar nitrogen concentrations of 3.8 and 4.2 at.%, respectively, were measured. This is expected as the diamond structure is not much affected under these conditions. However, these concentrations are significantly larger than those measured for H-Di(111) of ~0.5 and 1.5 at.% and H-Di(100) of ~1.25 and 0.8 at.% (respectively). It is suggested that the larger values measured for the H-MND surfaces are associated to the larger NH(ads) concentration as compared to the single crystal (SC) (and polycrystalline) surfaces, as could be determined by our HREELS measurements (section 3.2 below). This effect is possibly related to the larger density of H(ads) onto the H-MND surfaces as compared to the SC and PCD surfaces as determined by the spectral component of the C(1s) XP line shape associated to CH bonding and discussed in section 3.3 (see SI – Figure S4).

From Figure 1(a), following MW(N_2) exposure of the H-MND surface, nitrogen was nearly stable up to an annealing temperature of 500 °C and linearly decreased at higher annealing temperatures. A similar dependence was found for the H-Di(111) and H-Di(100) (as well as for PCD) surfaces. This similarity shows that the H-MND surfaces display similar properties to the single crystal cases.

The nitrogen thermal stability following RF(N_2) non-damaging H-MND surface, monotonically decreasing with annealing temperature, seems to be lower than those measured for the H-Di(111) and H-Di(100) surfaces. Whereas for the H-Di(100)[10, 11], it was found to be stable up to 700 °C and decreased at higher annealing temperatures; for the H-Di(111)[12, 13]

surfaces, it was found to be stable only up to 500 °C and decreased at higher temperatures. This difference may be associated to the higher concentration of NH(ads) species on the H-MND surfaces that display a lower thermal stability than CN(ads) species. Further studies are necessary to support this proposition.

The nitrogen thermal stability on the H-Di(100) and H-Di(111) single crystal surfaces for the non-damaging RF(N_2) and MW(N_2) exposure cases, for which very little damage is caused to the diamond surface, have been modeled by us previously and found to be associated to particular surface bonding configurations and in agreement with our experimental findings.[11, 13] In the case of damaging RF(N_2), nitrogen is likely to be bonded onto a disordered surface and near-surface region that display much lower temperature stability due to nitrogen bonding to defective carbon, promoting nitrogen desorption at lower temperatures.

From Figure 1(b), the oxygen concentration on the H-MND and MW(H_2)-MND samples at RT and after annealing to 300 °C before exposure to the nitrogen plasma were similar and obtained a value of ~2.5 at.%. A similar oxygen concentration was previously reported for annealed H-MND drop-casted films.[5] Also, from Figure 1(b), the damage and non-damage RF(N_2)-H-MND plasma exposed surfaces obtained similar values of ~2.1 at.%. Surprisingly, the oxygen concentration of the MW(N_2)-MND exposed surface at RT obtains a value of ~4.2 at.%. Then, the oxygen concentration monotonically decreased for all surfaces with annealing temperature.

In contrast, from our previous studies,[15] the H-Di(100), H-Di(111), and H-PCD surfaces exposure to different nitrogen plasmas, subsequent ambient exposure resulted in slightly lower oxygen adsorption. In that case, a larger intake, ~2.8 at.%, occurred for the damaging RF(N_2) exposure. Whereas for the MW(N_2) and non-damaging RF(N_2) plasma exposures, it was ~0.8 and ~1.3 at.%, respectively.[15] In the case of H-MND, the large oxygen concentration measured for the as-prepared drop-casted films is likely to be associated with the preparation process that involves sonication in water[5] or naturally occurring defects on the MND surfaces. Also, the faceted milled nano-diamond particles likely exhibit highly reactive grain edges compared to the poly and single crystalline surfaces, thus resulting in a higher adventitious oxygen intake. It is noticed that the thermal stability of the adventitious oxygen is similar for all studied surfaces: it monotonically decreases with annealing temperature as expected for oxygen bonding to defects on diamond surfaces.

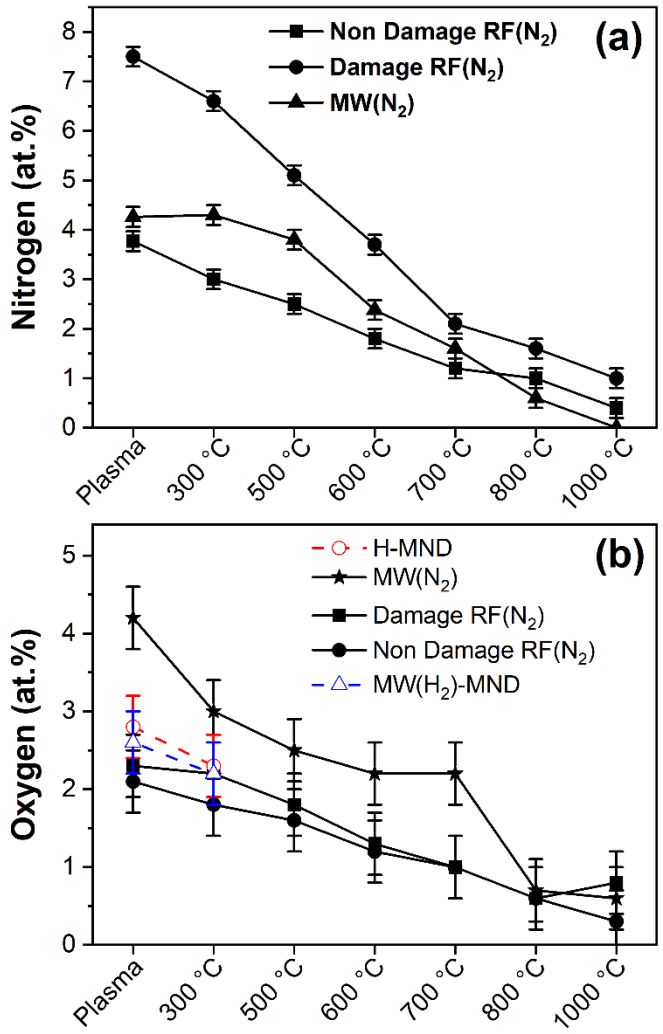

Figure 1. (a) nitrogen and (b) oxygen concentration following nitrogen plasma exposure and subsequent exposure to ambient conditions and annealing as calculated from the XPS survey.

3.1 Nitrogen Bonding and Thermal Stability and Surface Defects of Plasma Nitride H-MND Surface: C(1s) and N(1s) XP Line Shape Analysis

Below, a detailed spectroscopic analysis of the nitrogen and carbon-associated XP lines is presented to assess nitrogen bonding on the MND surfaces and near-surface structural damage induced by the different surface-plasma interactions. First, the adventitious oxygen bonding configuration on different surfaces and following annealing is shortly discussed. The oxygen bonding to the different surfaces was assessed from their O(1s) XP line shapes (not shown). For the H-MND annealed to 300 °C, the O(1s) was measured at 532.7 ± 0.2 eV eV. This suggests that adventitious oxygen is bonded in mainly C–O(ads) bonding configuration on pristine H-MND surfaces. For the MW(N_2) and RF(N_2) plasma exposed surfaces, the O(1s) position was measured at ~532.5 and 532.0 ± 0.2 eV, suggesting that following the plasma exposure, oxygen remains in a mainly C–O(ads) bonding configuration. This is further

corroborated by HREELS, where the absence of 220 meV peak, associated with C=O stretching mode, evidences no such species formation.

Following vacuum annealing up to 1000 °C of all plasma nitrogen-terminated H-MND surfaces, the O(1s) was measured at ~532 eV. It monotonically decreased in intensity, whereas its lineshape did not significantly change. Therefore, no evidence of NO_x(ads) bond formation on nitrogen-terminated and annealed surfaces was identified by XPS analysis.

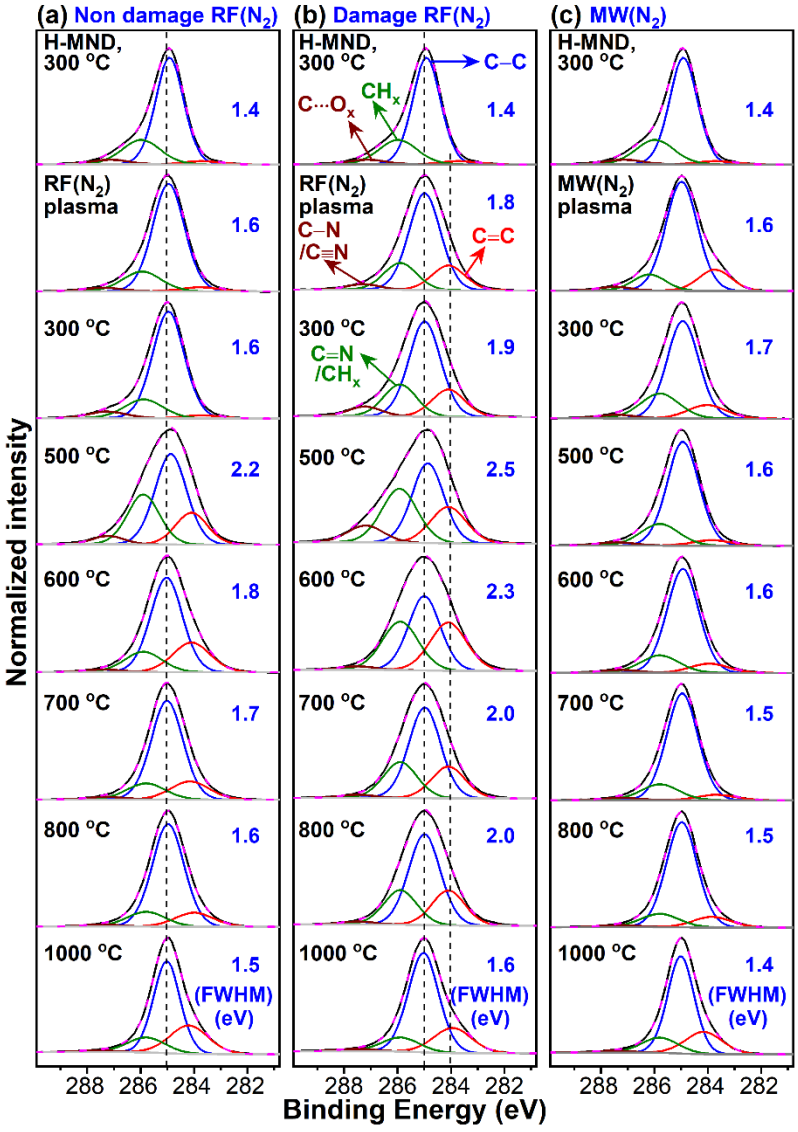

Figure 2. C(1s) core level spectra of H-MND surfaces exposed to different N_2 plasmas and stepwise annealed at various temperatures.

The nitrogen bonding configuration was derived from analyzing the N(1s) XP line shapes. Analysis of the C(1s) XP line shape was used to examine the evolution of defects on the surface by the plasma interaction. The C(1s) XP line shape measured for as-nitrided samples and after stepwise annealing are shown in Figure 2. For the H-MND and MW(H_2)-MND (annealed at

300 °C), an asymmetric C(1s) line centered at 285.0 ± 0.1 eV (FWHM = 1.5 eV) was measured. Fitting revealed four C(1s) spectral components: a minor component at 283.4 ± 0.2 eV associated with sp^2-hybridized carbon and non-diamond species (C=C),[19] a central peak at 285.0 ± 0.2 eV associated with sp^3-hybridized carbon (C–C),[20, 21] a significant component at 286.0-286.5 eV associated with CH_x species due to hydrogen bonding to surface carbon,[19] and a very-low intensity peak at 287.2 ± 0.2 eV ascribed to oxygen bonding to surface carbon atom in C···O_x state,[19, 22] which is due to partial oxidation of sample surface during sonification and sample transfer into the UHV chamber.

Upon exposure of the H-MND and MW(H_2)-MND surface to the RF(N_2) and MW(N_2) plasmas, the C(1s) XP line shape displays several changes. It should be mentioned that slight variations in C(1s) BE position up to ~-1 eV were observed following nitrogen plasma exposure. These shifts are associated with surface band bending and charging effects upon nitridation. The C–C component intensity decreased slightly; in contrast, the C=C component increased significantly. Fitting displays that the intensity of 286.0 eV and 287.2 ± 0.2 eV peaks increased upon nitridation and these peaks are ascribed to C=N(ad) besides CH_x and C–N(ad)/C≡N(ad) bonds, including partial C···O_x, respectively[22]. The CN assignments presented here are considered according to earlier reports on electron spectroscopic analysis of amorphous CNH_x films.[23] No further discussion is presented on the low-intensity C(1s) peaks related to CN bonds.

The damage induced by the plasma exposure to the H-MND near-surface region may be evaluated by monitoring the relative intensity of C(1s)-C=C spectral component for different plasma treatments and subsequent stepwise annealing. From Figure 2, it may be calculated that the C=C spectral intensity relative % concentration is similar and obtains a value of 1.5-2.5 % for the H-MND and MW(H_2)-MND samples. A similar value was recently reported from XPS analysis of H-MND.[5] Then, following exposure to the nitrogen plasmas, the intensity of the C=C spectral component increases, and its intensity follows the trend: RF(N_2) damage > RF(N_2) non-damage ~ MW(N_2) plasma exposure. In addition, the FWHM of the C(1s) XP peak, as derived from the casaXPS program, increases from a value of 1.4 eV upon exposure to the nitrogen plasma, obtaining a maximum value upon annealing to 500-700 °C and then decreases at higher annealing temperatures and obtaining similar values of 1.5 eV. The measured FWHM is shown next to each C(1s) XP peak in Figure 2. Also, in this case, the largest FWHM was measured upon damage RF(N_2), followed by non-damage RF(N_2) and

MW(N_2) plasma exposure. These results show the complex chemical nature of the nitrogen plasma exposed H-MND faceted surfaces.

Figure 3 displays the N(1s) spectra recorded from different nitrogen plasma exposed H-MND surfaces. In Figure 3, N(1s) spectra line shape and intensity display sharp contrast for different plasma exposed samples, indicating the population of various nitrogen bonding configurations. Next to each N(1s) XP peak, the FWHM is denoted.

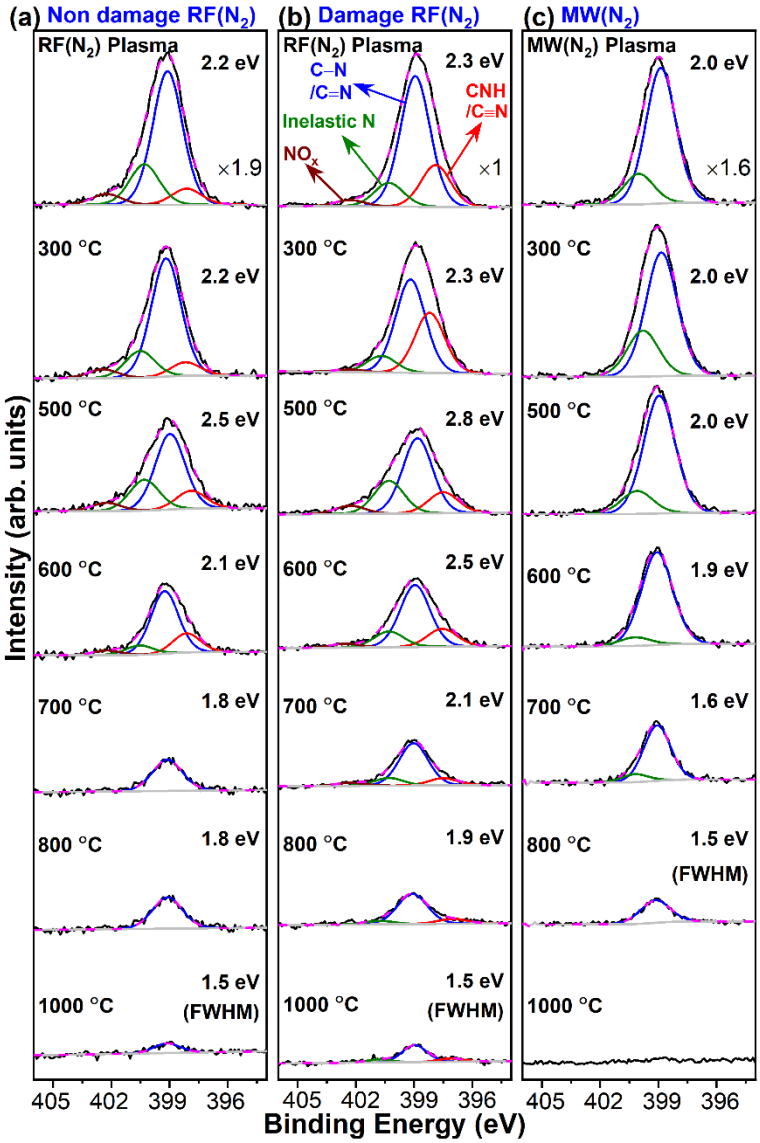

Figure 3. N(1s) core level spectra of H-MND surfaces exposed to different N_2 plasmas and subsequently annealed at various temperatures.

For the nitrogen-terminated surface produced by MW(N_2) plasma exposure (Figure 3, column (c)), the measured N(1s) XP peak was almost symmetric and centered at ~399 eV with an FWHM of 2.0 eV. Fitting shows a central peak at ~399 eV associated with C–N/C=N like

bonds and a low-intensity peak at ~400.8 ± 0.2 eV related to quaternary nitrogen or/and inter-band transition, as assigned earlier.[11, 13] The N(1s) XP peak intensity decreases with increasing annealing temperature without a change in its position, indicating nitrogen desorption and no other CN states evolved with annealing. From this figure, the FWHM of this peak monotonically decreases with annealing temperature: it obtains a value of 2.0 eV till 500 °C, which reduces to 1.9 eV upon annealing to 600 °C, 1.6 eV upon annealing to 700 °C and 1.5 eV upon annealing to 800 °C.

For the RF(N_2) (non-damaging) plasma exposure (Figure 3, column (a)), the N(1s) XP peak could be deconvoluted in three main spectral components at ~398 eV, ~399 eV, and 400.8 eV associated with C≡N, C–N/C=N and quaternary nitrogen.[8, 10-12] In our previous studies, the C≡N-like bonds are associated with nitrogen species bonded to structural defects in the diamond structure. Therefore, its relative intensity indicates the level of structural damage produced by the plasma-surface interaction. In this case, the FWHM of the N(1s) XP line was measured to be 2.2 eV following plasma exposure, increasing to 2.5 eV upon annealing to 500 °C and decreasing to 2.1 eV upon annealing to 600 °C and further decreases to 1.8 and 1.5 upon annealing to 800 °C and 1000 °C, respectively.

For the RF(N_2)(damaging) plasma exposure (Figure 3, column (b)), the N(1s) XP peak could be deconvoluted in three main spectral components at ~398 eV, ~399 eV, and 400.8 eV. As expected, the C≡N component in these cases is more significant than the others. Following plasma exposure, the FWHM of the N(1s) XP line was measured to be 2.2 eV; it increased to 2.8 eV upon annealing to 500 °C and decreased to 2.5 eV upon annealing to 600 °C and further decreased to 1.9 and 1.5 upon annealing to 800 °C and 1000 °C, respectively.

From the N(1s) spectral analysis, it is evident that for the as-exposed surfaces (Figure 3 - first spectrum in each column), the largest relative intensity of the spectral components associated with nitrogen bonding to defects, C≡N, was found for the RF(N_2) damaging case, followed by the RF(N_2) non-damaging case; whereas for the MW(N_2) it was absent. Furthermore, with annealing temperature, this component was found to decrease in relative intensity alongside a decrease in the FWHM till a final value of 1.5 eV for all three cases for annealing temperature in the 800-1000 °C range (Figure 3, last spectrum in each column). These results indicate that the nitride surfaces are composed of multiple nitrogen bonding configurations of different thermal stability. It is likely that in these cases a single bonding nitrogen configuration is populated on the H-MND nitride surfaces.

3.2 Hydrogen Bonding, Thermal Stability and Recovery of the Nitride Surfaces: HREELS Measurements

The question of hydrogen bonding on the H-MND surfaces before and after nitridation is investigated by HREELS. From this analysis, questions related to its bonding configuration before and following nitrogen plasma exposure and annealing are discussed. In Section-S2 in SI, HREELS measurements and peaks assignments of well-defined (as possible) different H-terminated diamond surfaces, including H-Di(100), H-Di(111), H-PCD, H-MND and MW(H_2)-MND surfaces are shown. Below, the HREEL spectra of nitrogen-terminated H-MND surfaces by different plasma exposures are described and analyzed.

3.2.1. HREELS Measurements of the Non-Damage Rf(N_2) Plasma Exposed H-MND Surface

The HREEL spectra of non-damaging RF(N_2) plasma exposed H-MND followed by stepwise annealed surfaces are shown in Figure 4(a) and (b). From Figure 4(a), the HREEL spectrum obtained from the as-nitride surface displays a broader 155 meV peak and low-intensity first-order optical phonon feature compared to pristine H-MND surface, suggesting that nitrogen adsorption onto H-MND significantly modifies carbon and hydrogen bonding locally. Also, from Figure 4(b), upon RF(N_2) plasma exposure at these conditions, an extra peak at 415-420 meV emerges in the spectrum. This indicates the population of –NH species on the H-MND surfaces, as previously found for the nitride H-Di(111), H-Di(100), and H-PCD surfaces.[9] The 415-420 meV peak disappeared after 700 °C annealing and the spectrum resembles H-MND spectrum, indicating significant surface recovery. Curve-fitting of the 155 meV peak unveils a rise in C=C content and the population of C=N bonds on the surface (indicated in a blue-dashed circle), which exhibit thermal stability above 700 °C. XPS analysis shows the presence of ~1 at.% of nitrogen on the 700 °C annealed surface (possibly single bonding state). It is interesting to note that the intensity of the -NH stretching mode at 415-420 meV is much more prominent in this case than that measured for the H-PCD, H-Di(100), and H-Di(111) surfaces following the same plasma nitridation process previously published by us.[8, 9, 13] This difference is further discussed below.

As can be seen from Figure 4, the spectral component of the CH peak associated with H bonding to H-Di(111) facets disappears upon exposure to the nitrogen plasma (spectra 1 and 2 in Figure 4). Only the spectral component associated with H bonding to the H-Di((100) and defects could be measured in the spectrum. This effect was observed in our previous study of

nitrogen plasma interaction with the H-Di(111) surface: the CH peak shifted from 350 to 360 meV upon nitrogen interaction.[13] This effect was explained by DFT modeling, which shows that the CH vibrational modes to the (111) surfaces are affected by neighboring NH adsorbates, resulting in the measured spectral shift.[13] Also, from spectrum-5 in Figure 4, upon -NH desorption (decreases of the 415-420 meV peak) upon annealing to 600 °C, the spectral component associated with H bonding to the (111) facets is recovered – while with slightly lower intensity compared to the H-MND surface.

Upon annealing to 1000 °C, the HREEL displays the first and second order ν(C–C) overtone but at a lower relative intensity to that measured for the H-MND annealed to 300 °C (spectrum 1 in Figure 4), suggesting that upon annealing to 1000 °C a nearly recovered H-MND surface was obtained. These results show that no significant damage was induced to the H-MND surface by the nitridation process.

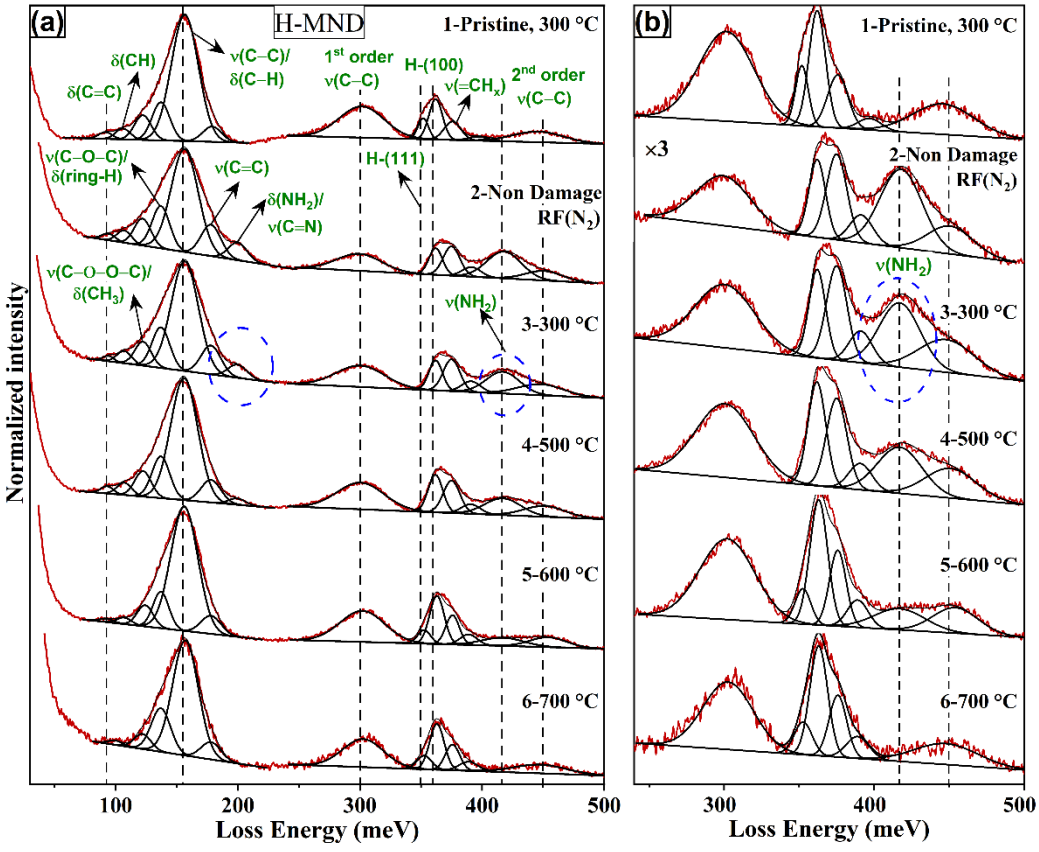

Figure 4. (a) HREEL spectra of H-MND surface exposed to non-damage RF(N_2) plasma and subsequently annealed at different temperatures. (b) ×3 magnified (in the y-axis) spectra of (a) in the range 230–500 meV.

3.2.2. HREELS Measurements of the Damage RF(N_2) Plasma Exposed H-MND Surface

The HREELS spectra of damaging RF(N_2) plasma exposed H-MND followed by stepwise annealed surfaces are shown in Figure 5(a) and (b). From Figure 5(a), in this case, the HREEL spectrum of as-nitride surface displays a very wider 155 meV peak, and the first-order ν(C–C) overtone peak is absent from the spectrum compared to pristine H-MND surface, indicating that nitrogen incorporation onto H-MND extensively modifies local carbon and hydrogen bonding and induce considerable damage to MND. Also, from Figure 5(b), upon RF(N_2) plasma exposure at these conditions, the peak at 415-420 meV is much more intense, which suggests the presence of a higher concentration of –NH species as compared to the non-damaging RF(N_2) plasma exposure and corroborating the observed higher nitrogen concentration for RF(N_2) damaging plasma exposed surfaces obtained from our XPS analysis. Upon annealing to 700 °C, the ~420 meV was not measured, suggesting that associated species fully desorbed from the surfaces at this temperature NH. Following annealing to 700 °C, no recovery of the first and second order ν(C–C) overtones was measured for this case. From a wider 155 meV peak, it can be noticed that the C=C and C=N content on the surface is significantly larger compared to the non-damaging RF(N_2) conditions. These observations showed that following these plasma exposure conditions, a pronounced deterioration of the diamond surface occurred that could not be recovered upon high-temperature annealing. This agrees with the C(1s) XP peak spectral analysis conclusions. XPS analysis shows the presence of ~5 at.% nitrogen on the 700 °C annealed surface. Upon annealing to 1000 °C, the HREEL does not display the first and second order ν(C–C) overtone, suggesting that annealing to 1000 °C did not result in recovery of the H-MND surface and a graphitized near-surface region was produced.

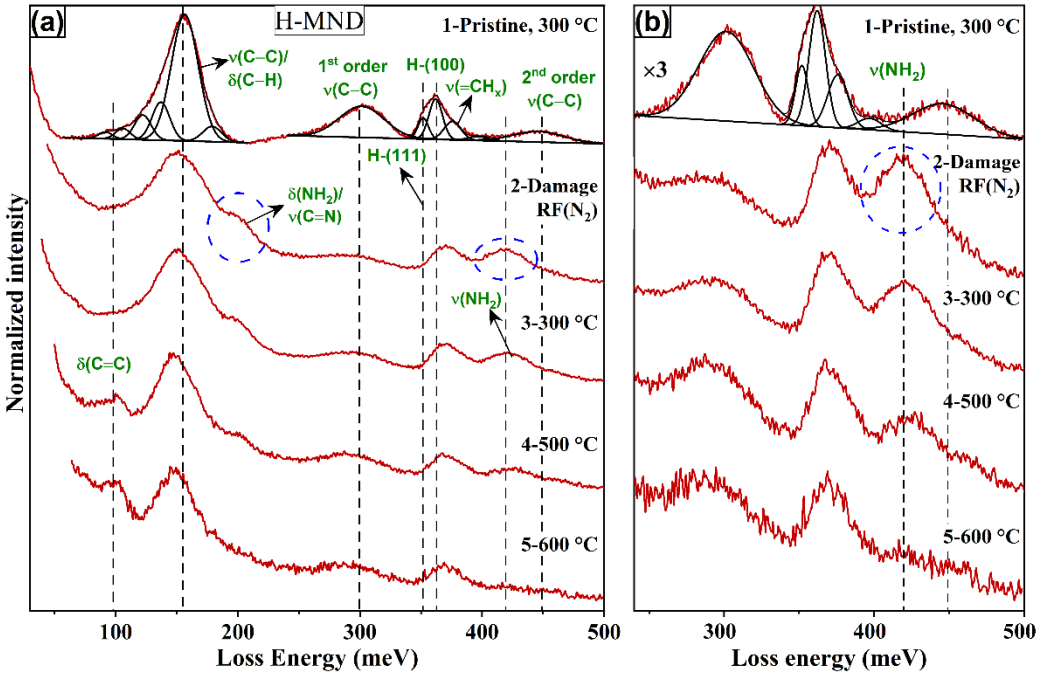

Figure 5. (a) HREEL spectra of H-MND surface exposed to damage RF(N_2) plasma and subsequently annealed at different temperatures. (b) ×3 magnified (in the y-axis) spectra of (a) in the range 230–500 meV.

3.2.3. HREELS Measurements of the MW(N_2) Plasma Exposed MW(H_2)-MND Surface

The HREELS spectra obtained from the as-MW(N_2) plasma exposed MW(H_2)-MND followed by stepwise annealed surfaces are shown in Figure 6(a) and (b). From Figure 6(a), the HREEL spectrum of as-nitride H-MND surface displays very broad 155 and 360 meV peaks. The intensity of first order ν(C–C) overtone decreased compared to the M(H_2)-MND surface. From Figure 6(b), for MW(N_2) plasma exposed surface, a minor extra peak at 415-420 meV emerges in the spectrum. This indicates the population of –NH species on the H-MND surfaces, as previously found for the RF nitride surfaces. Upon annealing to 600 °C, the 415-420 meV peak strongly decreases in intensity. However, it could still be measured upon annealing at 700°C.

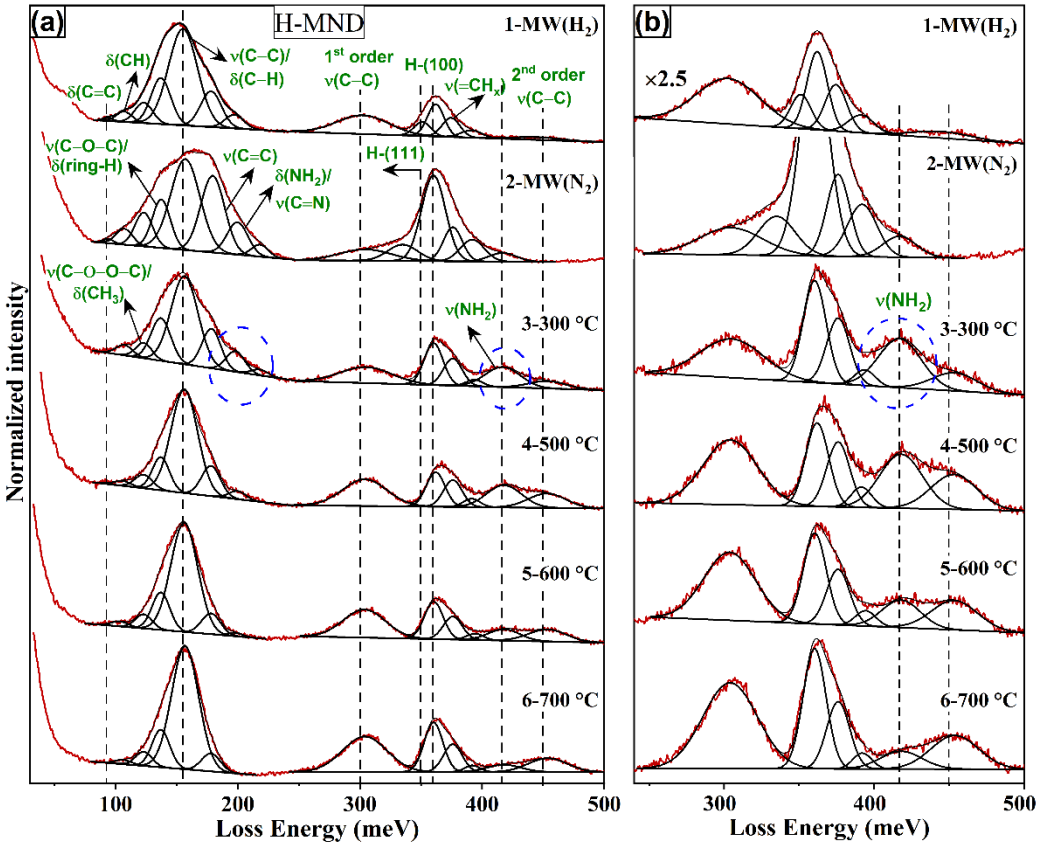

Figure 6. (a) HREEL spectra of MW(H_2)-MND surface exposed to MW(N_2) plasma and subsequently annealed at different temperatures. (b) ×2.5 magnified (in the y-axis) spectra of (a) in the range 230–500 meV.

From the HREELS measurements conducted for the different studied surfaces, it can be inferred that nitrogen and hydrogen co-exist on all plasma-nitrided surfaces studied and adventitious oxygen bonded in various configurations in agreement with the XPS analysis. All HREEL spectra of N_2 plasma exposed surfaces displayed =CH vibrational states and observed broadening of ~150 meV, demonstrating the formation of various CN species and defects/damage (sp^2-hybridized carbon (C=C)) nitrided surfaces. Especially, appeared a peak at 415-420 meV, which is assigned to an NH_x stretching mode, previously reported by us.[9, 13]

After annealing the RF(N_2) plasma exposed surfaces to 600-700 °C, the disappearance of 415-420 meV peak, assigned to NH_x stretching mode, from the spectra, indicating either thermal dissociation of NH_x species leading to H(ads) and N(ads) species or desorption of NH_x species. XPS analysis reveals a significant decrease in nitrogen content in the 600-700 °C range. The preferred explanation is the desorption of NH_x species, as it decreases the N(1s) peak intensity as well. Further experiments are necessary to elucidate and discern between these two possibilities.

3.3 Influence of Hydrogen on Nitrogen Bonding

A comparison is made of the relative intensity of the -NH(ads) vibrational band at 415-420 meV measured for the H-MND, H-PCD, and H-Di(100) surfaces following RF(N_2) non-damaging and MW(N_2) plasma exposure. In Figure 7, the relative intensity of the -NH (ads) vibrational band to the -CH(ads) vibrational band at 360 meV are plotted for these nitrided surfaces and as a function of annealing temperature. This comparison shows that the -NH(ads) population on the MND surfaces is much higher than on the PCD and Di(100) surfaces. It may be suggested that this effect is associated to the larger adsorption sites available to form -NH(ads) bonds. An indication that this is the case may originate from the relative intensity of the C(1s) XP spectral components associated with CH to the total C(1s) XP peak shown in Figure S4 in SI. In Figure S4, the C(1s) -XP spectra measured for the H-Di(100), H-PCD and H-MND following in vacuum annealing processes as those applied before the RF(N_2) non-damaging nitridation process are shown. From the values shown in Figure S4, the relative increase in the CH spectral component between the H-MND and the H-PCD surfaces is ~2.44 (=22.2/9.1) (Figure S4), whereas the relative increases in the -NH(ads) vibrational modes upon RF(N_2) non-damaging and annealing to 300 °C between these two surfaces is ~2.5 (40/16) (Figure 7). A similar calculation between the H-MND and the H-Di(100) renders values of 2.9 (=22.6/7.6) for the CH spectral component and 5 (=40/8) for the -NH mode. These comparisons may support our proposition; however, further studies are necessary to justify it.

From Figure 7, in all cases, annealing in 600-700 °C range results in a pronounced decrease in the relative intensity of -NH(ads) band, which may be associated with H desorption and N bonding to the surface or desorption of the NH species. These results suggest a very similar nature of bonding of the NH species to the diamond surfaces. As from our XPS analysis, the nitrogen concentration decreases in this temperature range. It is suggested that -NH species desorb in this temperature range. This would result in a more homogenous nitrogen bonding to the MND surfaces as reflected by the decreases in the FWHM of the N(1s) XP peak measured upon annealing to 700 °C and above for all nitride surfaces (Figure 3).

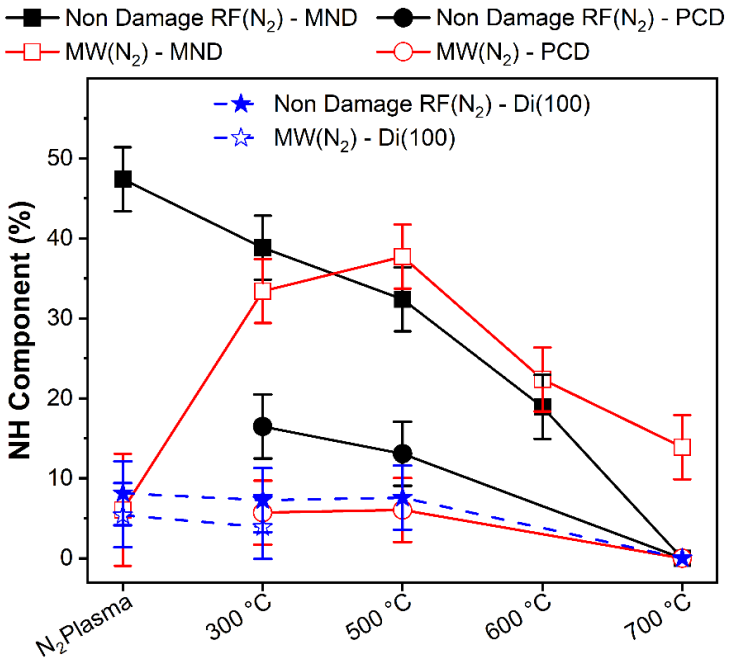

Figure 7. Relative intensity (%) of the NH vibrational mode at 415-420 meV to the CH vibrational mode at 360 meV for the different plasma nitride MND, PCD, and Di(100) samples.

Another general feature of our HREELS measurements of the different surfaces is the absence –OH (ads) vibrational modes. This suggests that the adventitious oxygen is bonded directly to C sites, albeit possibly in different bonding configurations. Furthermore, as no vibrational mode was observed at ~220 meV, it can be concluded that no C=O-like bonds are formed between the adventitious oxygen and the diamond surface.

4. Summary

The nitrogen and oxygen concentration and thermal stability of different plasma nitrogen-terminated H-MND drop-casted film surfaces were investigated. The highest amount of adsorbed nitrogen of ~7.5 at.% was for the damaging RF(N_2) plasma-treated surface, followed by the MW(N_2) and non-damaging RF(N_2) plasma-treated surfaces with nitrogen concentrations of 4.2 and 3.8 at.%, respectively. The thermal stability of the adsorbed nitrogen and oxygen was measured, and it was found to decrease with annealing temperature in the 300-1000 °C range.

From N(1s) spectral analysis, MW(N_2) plasma exposure populates C–N/C=N bonded species predominantly, leading to a symmetric and narrow N(1s) spectrum. Whereas damage RF(N_2) plasma exposure leads to the formation of C≡N (nitrile-like) (N bonded to carbon defects induced by plasma-surface interaction) significantly besides C–N/C=N states.

Our XPS measurements show that most of the adventitious oxygen is adsorbed in a CO_x configuration, whereas HREELS measurements show that no C=O(ads) or OH(ads) species are formed on the surface upon exposure of the nitride surfaces to ambient conditions. The HREELS analysis shows that the hydrogen adsorbed on the MND surfaces is not removed by exposure to the different nitrogen plasmas. These measurements show that NH(ads) species are formed on the surface and are desorbed upon vacuum annealing in the 500-700 °C range. The appearance of the second optical overtone at 450 meV in the HREEL spectra of the RF(N_2) non-damaging exposed surface upon annealing to 1000 °C suggests that this is mostly structurally recovered upon nitrogen desorption and annealing. In contrast, the MW(N_2) exposed diamond surface displayed some surface damage. Severe surface damage was induced to the diamond surface upon exposure to damaging RF(N_2) plasma. These conclusions are corroborated by C(1s) spectral analysis.

The results of this study suggest that the population of NH(ads) species on the H-MND surfaces following the different plasma exposures and annealing processes is larger than that for the PCD and SC surfaces following similar treatments. However, in-vacuum thermal annealing results in a pronounced desorption of these species and recovery of the H-MND surfaces.

Supporting Information

Structural and morphological characterization of the H-MND samples by electron microscopy.

Chemical properties of the H-MND surfaces by NEXAFS, XPS, and HREELS.

Acknowledgments

We want to thank Technion-IIT for the promotion of research. We would also like to thank Helen Diller Quantum Center, Technion, for supporting this work financially. This research was supported by the ISRAEL SCIENCE FOUNDATION (Grant No. 557/23). We thank Helmholtz-Zentrum Berlin (HZB) for the allocation of synchrotron radiation beamtime at HZB (Germany) as well as Maria Brzhezinskaya for the beamline support. This study is funded by a Freigeist Fellowship from the Volkswagen Foundation (No 89592). AC and TD thank the CEA for funding the PhD of MF.

References

(1) Girard, H. A.; Arnault, J.-C. Tuning Surface Properties of Detonation and Milled Nanodiamonds by Gas Phase Modifications. In *Novel Aspects of Diamond II: Science and Technology*, Mandal, S., Yang, N. Eds.; Springer Nature Switzerland, 2024; pp 47-76.

(2) Stehlik, S.; Mermoux, M.; Schummer, B.; Vanek, O.; Kolarova, K.; Stenclova, P.; Vlk, A.; Ledinsky, M.; Pfeifer, R.; Romanyuk, O.; et al. Size Effects on Surface Chemistry and Raman Spectra of Sub-5 nm Oxidized High-Pressure High-Temperature and Detonation Nanodiamonds. *J. Phys. Chem. C* **2021**, *125* (10), 5647-5669. DOI: https://doi.org/10.1021/acs.jpcc.0c09190.

(3) Ajoy, A.; Nazaryan, R.; Druga, E.; Liu, K.; Aguilar, A.; Han, B.; Gierth, M.; Oon, J. T.; Safvati, B.; Tsang, R.; et al. Room temperature "optical nanodiamond hyperpolarizer": Physics, design, and operation. *Rev. Sci. Instrum.* **2020**, *91* (2), 023106. DOI: https://doi.org/10.1063/1.5131655.

(4) Miliaieva, D.; Djoumessi, A. S.; Čermák, J.; Kolářová, K.; Schaal, M.; Otto, F.; Shagieva, E.; Romanyuk, O.; Pangrác, J.; Kuliček, J.; et al. Absolute energy levels in nanodiamonds of different origins and surface chemistries. *Nanoscale Adv.* **2023**, *5* (17), 4402-4414. DOI: http://dx.doi.org/10.1039/D3NA00205E.

(5) Saoudi, L.; Girard, H. A.; Larquet, E.; Mermoux, M.; Leroy, J.; Arnault, J.-C. Colloidal stability over months of highly crystalline high-pressure high-temperature hydrogenated nanodiamonds in water. *Carbon* **2023**, *202*, 438-449. DOI: https://doi.org/10.1016/j.carbon.2022.10.084.

(6) Krueger, A. Chapter 8 - Current issues and challenges in surface chemistry of nanodiamonds. In *Nanodiamonds*, Arnault, J.-C. Ed.; Elsevier, 2017; pp 183-242.

(7) Malkinson, R.; Kuntumalla, M. K.; Chemin, A.; Petit, T.; Hoffman, A.; Bar-Gill, N. Enhanced quantum properties of shallow diamond atomic defects through nitrogen surface termination. *J. Mater. Chem. C* **2024**, *12* (20), 7206-7213. DOI: http://dx.doi.org/10.1039/D4TC00581C.

(8) Kuntumalla, M. K.; Attrash, M.; Li, F.; Hoffman, A. Influence of RF(N_2) plasma conditions on the chemical interaction and stability of activated nitrogen with polycrystalline diamond

surfaces: A XPS, TPD and HREELS study. *Surf. Sci.* **2019**, *679*, 37-49. DOI: https://doi.org/10.1016/j.susc.2018.08.019.

(9) Attrash, M.; Kuntumalla, M. K.; Michaelson, S.; Hoffman, A. Nitrogen-terminated polycrystalline diamond surfaces by microwave chemical vapor deposition: Thermal stability, chemical states, and electronic structure. *J. Phys. Chem. C* **2020**, *124* (10), 5657-5664. DOI: https://doi.org/10.1021/acs.jpcc.9b10829.

(10) Attrash, M.; Kuntumalla, M. K.; Hoffman, A. Bonding, structural properties and thermal stability of low damage RF(N_2) plasma treated diamond (100) surfaces studied by XPS, LEED, and TPD. *Surf. Sci.* **2019**, *681*, 95-103. DOI: https://doi.org/10.1016/j.susc.2018.11.006.

(11) Zheng, Y.; Kuntumalla, M. K.; Attrash, M.; Hoffman, A.; Huang, K. Effect of Surface Hydrogenation on the Adsorption and Thermal Evolution of Nitrogen Species on Diamond(001) by Microwave N_2 Plasma. *J. Phys. Chem. C* **2021**, *125* (51), 28157-28161. DOI: https://doi.org/10.1021/acs.jpcc.1c09514.

(12) Attrash, M.; Kuntumalla, M. K.; Michaelson, S.; Hoffman, A. Nitrogen terminated diamond (111) by RF(N_2) plasma – chemical states, thermal stability and structural properties. *Surf. Sci.* **2021**, *703*, 121741. DOI: https://doi.org/10.1016/j.susc.2020.121741.

(13) Kuntumalla, M. K.; Zheng, Y.; Attrash, M.; Gani, G.; Michaelson, S.; Huang, K.; Hoffman, A. Microwave N_2 plasma nitridation of H-diamond (111) surface studied by ex situ XPS, HREELS, UPS, TPD, LEED and DFT. *Appl. Surf. Sci.* **2022**, *600*, 154085. DOI: https://doi.org/10.1016/j.apsusc.2022.154085.

(14) Kawai, S.; Yamano, H.; Sonoda, T.; Kato, K.; Buendia, J. J.; Kageura, T.; Fukuda, R.; Okada, T.; Tanii, T.; Higuchi, T.; et al. Nitrogen-Terminated Diamond Surface for Nanoscale NMR by Shallow Nitrogen-Vacancy Centers. *J. Phys. Chem. C* **2019**, *123* (6), 3594-3604. DOI: https://doi.org/10.1021/acs.jpcc.8b11274.

(15) Kuntumalla, M. K.; Hoffman, A. Influence of Different Nitrogen Plasmas Exposures of H-Diamond (100) Surfaces on Ambient Oxygen Adsorption, Nitrogen Bonding, and Thermal Stability Studied by X-Ray Photoelectron Spectroscopy. *Phys. Status Solidi A* **2024**, *221* (8), 2300319. DOI: https://doi.org/10.1002/pssa.202300319.

(16) Michaelson, S.; Lifshitz, Y.; Hoffman, A. High resolution electron energy loss spectroscopy of hydrogenated polycrystalline diamond: Assignment of peaks through modifications induced by isotopic exchange. *Diamond Relat. Mater.* **2007**, *16* (4), 855-860. DOI: https://doi.org/10.1016/j.diamond.2006.11.079.

(17) Shirley, D. A. High-Resolution X-Ray Photoemission Spectrum of the Valence Bands of Gold. *Phys. Rev. B* **1972**, *5* (12), 4709-4714. DOI: https://doi.org/10.1103/PhysRevB.5.4709.

(18) Moulder, J. F.; Stickle, W. F.; Sobol, P. E.; Bomben, K. D. *Handbook of X-ray photoelectron spectroscopy: A reference book of standard spectra for identification of XPS data*; Perkin-Elmer Corporation, 1992.

(19) Ghodbane, S.; Ballutaud, D.; Omnès, F.; Agnès, C. Comparison of the XPS spectra from homoepitaxial {111}, {100} and polycrystalline boron-doped diamond films. *Diamond Relat. Mater.* **2010**, *19* (5), 630-636. DOI: https://doi.org/10.1016/j.diamond.2010.01.014.

(20) Graupner, R.; Maier, F.; Ristein, J.; Ley, L.; Jung, C. High-resolution surface-sensitive C 1s core-level spectra of clean and hydrogen-terminated diamond (100) and (111) surfaces. *Phys. Rev. B* **1998**, *57* (19), 12397-12409. DOI: https://doi.org/10.1103/PhysRevB.57.12397.

(21) Dieckhoff, S.; Ochs, D.; Günster, J.; Kempter, V. Metastable impact electron spectroscopy (MIES) study of chemical vapour deposited (CVD) diamond films. *Surf. Sci.* **1999**, *423* (1), 53-60. DOI: https://doi.org/10.1016/S0039-6028(98)00894-2.

(22) Le Normand, F.; Hommet, J.; Szörényi, T.; Fuchs, C.; Fogarassy, E. XPS study of pulsed laser deposited CN_x films. *Phys. Rev. B* **2001**, *64* (23), 235416. DOI: https://doi.org/10.1103/PhysRevB.64.235416.

(23) Chemin, A.; Kuntumalla, M. K.; Brzhezinskaya, M.; Petit, T.; Hoffman, A. Depth profiling of microwave nitrogen-terminated polycrystalline diamond surfaces by energy-dependent X-ray photoelectron spectroscopy. *Appl. Surf. Sci.* **2024**, *661*, 160082. DOI: https://doi.org/10.1016/j.apsusc.2024.160082.

TOC Graphic

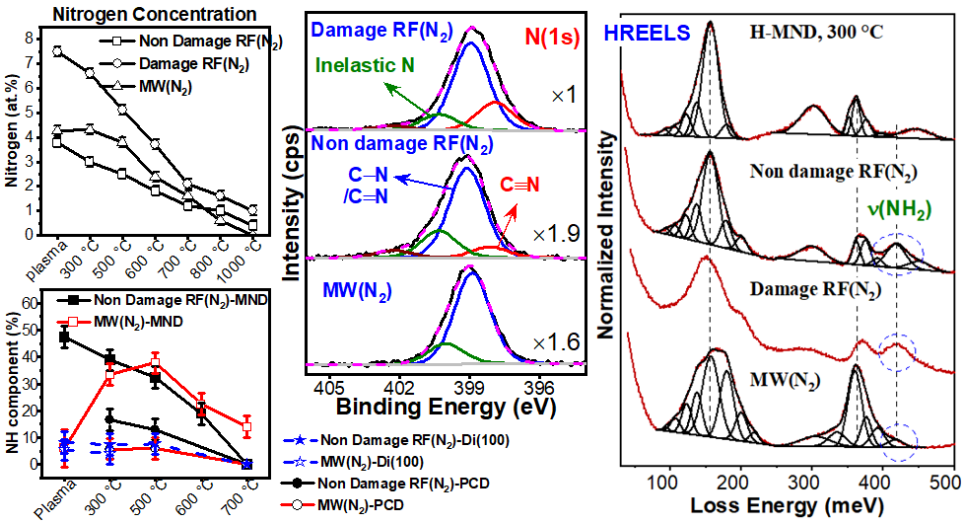
Nitrogen Concentration
Non Damage RF(N2)
Damage RF(N2)
MW(N2)
Nitrogen (at.%)
plasma
300 °C
500 °C
600 °C
700 °C
800 °C
1000 °C
Non Damage RF(N2)-MND
MW(N2)-MND
NH component (%)
Plasma
Damage RF(N2)
N(1s)
Inelastic N
×1
Non damage RF(N2)
C–N
/C=N
C≡N
×1.9
MW(N2)
×1.6
Intensity (cps)
405
402
399
396
Binding Energy (eV)
Non Damage RF(N2)-Di(100)
MW(N2)-Di(100)
Non Damage RF(N2)-PCD
MW(N2)-PCD
HREELS
H-MND, 300 °C
Non damage RF(N2)
ν(NH2)
Damage RF(N2)
MW(N2)
Normalized Intensity
100
200
300
400
500
Loss Energy (meV)